Article:

Guan, M, Wright, NG, Sleigh, PA et al. (1 more author) (2015) Assessment of hydro-morphodynamic modelling and geomorphological impacts of a sediment-charged jökulhlaup, at Sólheimajökull, Iceland. Journal of Hydrology, 530. 336 - 349. ISSN 0022-1694

https://doi.org/10.1016/j.jhydrol.2015.09.062

Assessment of hydro-morphodynamic modelling and geomorphological impacts of a sediment-charged jökulhlaup, at Sólheimajökull, Iceland

Mingfu Guan [a *], Nigel G. Wright [a], P. Andy Sleigh [a], Jonathan L. Carrivick [b]

[a] Water@Leeds and School of Civil Engineering, University of Leeds, Leeds, LS2 9JT, UK

[b] Water@Leeds and School of Geography, University of Leeds, Leeds, LS2 9JT, UK

Abstract: Understanding of complex flood-riverbed interaction processes in large-scale (field) outburst floods remains incomplete, not least due to a lack of well-constrained field data on hydraulics and sediment transport, but also because consensus on an appropriate model framework has yet to be agreed. This study presents a novel full 2D hydro-morphodynamic model containing both bedload and suspended load capability. Firstly, the model design is presented with an emphasis on its design to simulate rapidly-varied sediment-laden outburst floods and also the associated geomorphological impacts. Secondly, the model is applied to a large-scale (field) glacier outburst flood or 'jökulhlaup' at Sólheimajökull, Iceland. For this real-world event, model scenarios with only water and with inclusion of sediment with different parameter setups were performed. Results indicated that grain size specifications affected resultant geomorphological changes, but that the sensitivity of the simulated riverbed changes to the empirical bedload transport formulae were insignificant. Notably, a positive feedback occurred whereby the jökulhlaup led to significant net erosion of the riverbed, producing an increase in flow conveyance capacity of the river channel. Furthermore, bulking effects of sediment entrainment raised the peak discharge progressively downstream, as well as the flood volume. Effects of geomorphological changes on flood water level and flow velocity were significant. Overall, despite the increased computational effort required with inclusion of sediment transport processes, this study shows that river morphological changes cannot be ignored for events with significant in-channel erosion and deposition, such as during outburst floods.

Keywords: morphodynamic model; outburst floods; sediment transport; river morphology

* Corresponding author. Dr. Mingfu Guan
Email address: mingfu.guan@hotmail.com;

1. Introduction

Outburst floods or dam break type floods are amongst the most catastrophic natural hazards for human society and infrastructure. Part of the hazard of outburst floods is due to sediment transport. Glacial outburst floods or 'jökulhlaups' are a sudden onset flood from glaciers and ice sheets, either due to an ice or moraine dam failure, or due to volcanic or geothermal activity (Alho et al., 2005; Carrivick et al., 2010; Carrivick and Rushmer, 2006; Dai et al., 2005; Huggel et al., 2002; Manville et al., 1999). Field evidence demonstrates jökulhlaups often entrain a large amount of sediment and cause severe in-channel erosion and deposition, owing to high flow energy (Alho et al., 2005; Russell et al., 2010; Staines et al., 2014). In contrast to perennial river flows, a jökulhlaup is usually orders of magnitude larger in discharge, which implies that within a jökulhlaup the flood-riverbed interaction is more intense. In proglacial areas, the riverbed generally comprises of poorly sorted sediment materials from coarse particles (nominally greater than 250 mm) to fine (sand) particles (Alho et al., 2005; Russell et al., 2010), hence both bedload-dominant sheet flows and suspended load govern the sediment movement within a jökulhlaup. The entrained sediments will admittedly affect floodwater dynamics and rheology and riverbed adjustment (Berzi and Jenkins, 2008; Carrivick et al., 2011). However, the complex sediment - bed interactions within jökulhlaups are poorly understood, because of the difficulty of field measurements and the unpredictability of such sudden onset floods.

Partly as a reaction to the problem of field measurements, small-scale laboratory experiments (e.g. (Carrivick et al., 2011; Zech et al., 2008)) have been conducted and provide fundamental insights into the hydraulics and flow-bed interactions within dam break outburst floods. The studies have shown that gravel particles in outburst floods are generally transported in bedload dominant mode in a specific layer called a 'sheet flow layer'; while the finer particles are transported in a suspension layer. These experiments were performed in small-scale flumes with specific definition of flow conditions or grain-size distribution. The laboratory work therefore is only a crude model of geomorphological processes within large-scale outburst floods, because of the complexity of the real-world topography and flow conditions, spatially varying grain-size distribution, as well as the difficulty in ensuring physical similarity. In recent decades, attention has increasingly been paid to numerical modelling of such flood events (Carling et al., 2010; Carrivick et al., 2010); because it can give greater details of the phenomena during an event that cannot be captured by field and flume measurements. Although the exact quantification of bed change is unattainable through numerical modelling, the modelling technique can enhance and improve our insights into rapid sediment-laden floods (e.g. Carrivick et al., (2013).

In terms of numerical models, which should be informed by field data or experimental data, to date a large number of one-dimensional (1D) and two-dimensional (2D) morphodynamic models have been developed to represent erosion and deposition by dam-break outburst floods (Cao et al., 2004; Fraccarollo and Capart, 2002; Guan et al., 2015; Zech et al., 2008). However, these numerical models have been limited to theoretical investigations or to simulating small-scale laboratory flume experiments. Numerical modelling of a large-scale real-world flood with river morphology changes includes Carrivick et al. (2010) and Huang et al. (2014), but is still rare despite its being crucial to improving understanding of geomorphological processes with outburst floods and their complex interactions. Some fully three-dimensional (3D) morphodynamic models based on Navier-Stokes equations have also been reported in recent decades (Khosronejad et al., 2007; Shimizu et al., 1990; Wu et al., 2000). A 3D model can give more detailed computation of the water flow field, such as inclusion of secondary flows. However, a disadvantage in using a fully 3D model is that the computational time is at least an order of magnitude longer than a 2D model. The majority of the fully 3D models were developed focusing on meandering channel flows or flows near structures where complex 3D features are exhibited. Although there are studies to investigate the possibility of modelling the bed changes in a natural river using a fully 3D model (Fischer-Antze et al., 2008), these are still quite rare (Westoby et al., 2014). For engineering applications, a 2D hydro-morphodynamic model is usually adequate. The capabilities of 2D models include the ability to simulate multi-directional and multi-channel flows, super-elevation of flow around channel bends and turbulent eddying. These are dynamic characteristics intrinsic to a jökulhlaup and all types of outburst floods.

A 2D layer-based morphodynamic model has been developed and validated against a series of experimental tests for a noncohesive dyke breach (Guan et al., 2014). However, this model only accounted for uniform bedload, which is only applicable to cases of bedload-dominant sheet flows. Field evidence demonstrates that suspended load plays an equally important role for jökulhlaups (Carling, 2013; Staines, 2012). Therefore, building on the bedload dominant sheet flow model (Guan et al., 2014), an improved layer-based model is developed in this study by the inclusion of a suspended load model, and by including non-uniform sediment characteristics. Furthermore, this study applies the hydro-morphodynamic model to the well documented 1999 jökulhlaup in Iceland, to explore geomorpholocial impacts within the jökulhlaup. Therefore, the aims of this study are: (1) to develop a numerical model capable of modelling field-scale outburst floods with bedload and suspended load, and geomorphological changes, (2) to explore the effects of the morphological changes within a jökulhlaup on flood dynamics, and (3) to improve understanding of rapidly-varied and unsteady hydraulics and flow-bed interactions in large-scale jökulhlaups.

2. Study area and data collection

2.1. The 1999 jökulhlaup

Jökulhlaups induced by volcanic activity have frequently occurred in Iceland and one of them, the July 1999 jökulhlaup burst from Sólheimajökull southern Iceland. The 1999 jökulhlaup has been well recorded through field investigations (Russell et al., 2000; Russell et al., 2010; Sigurdsson et al., 2000; Staines, 2012; Staines et al., 2014), which provides a good opportunity to develop greater understanding of geomorphological impacts of a sediment-charged jökulhlaup through detailed numerical modelling. Sólheimajökull is an approximately 8 km long temperate, non-surging outlet glacier draining the Mýrdalsjökull ice cap belonging to the southern volcanic zone in Iceland (Fig. 1a). The glacier surface area is 78 km^2 with a snout 1 km wide, and it is slightly over-deepened. A river channel called Jökulsá á Sólheimasandi drains Sólheimajökull which has three main flow sources: (1) Jökulsárgilsjökull, an outlet glacier 3 km to the north of Sólheimajökull; (2) the glacial meltwater from Sólheimajökull itself via a 1km long subglacial tunnel; and (3) the river Fjallgilsá, flowing into the Jökulsá approximately 2 km downstream of the glacier snout.

The flooding process was sudden, short-lived and had high discharge, lasting approximately 6 h. The flood burst initially from the western margin of Sólheimajökull and drained into a former ice-dammed lake basin, approximately 3.7 km from the glacier snout thereby filling it (Fig. 1b location a). Then the meltwater overspill from this lake basin flowed into a lower tributary valley, Jökulsárgil (Fig. 1b location b). Additional floodwater increased the discharge into Jökulsárgil along the western margin of the glacier between the upper basin and Jökulsárgil, and meanwhile shattered glacial ice entered into Jökulsárgil with meltwater caused by ice fracturing. Additionally, the supra-glacial fracture outlets about 3km from the glacier snout also carried quantities of sediment-laden floodwater (Roberts et al., 2003). The Western Conduit and the Central Conduit were the two major floodwater sources in the river channel. The Western Conduit with 150 m in width was the biggest floodwater source, and the Central Conduit opened up in the centre of the snout draining the majority of waning stage and post-outburst flooding flow. The floodwater in the two conduits ran together into the river channel, Jökulsá á Sólheimasandi. Some smaller flows exited the eastern margin of the snout from a small, newly-cut, steep-sided channel and from a series of minor outlets flowing across vegetated hillslopes.

2.2. Data collection and general considerations

The data used in this study are summarised in Table 1. The bed terrains before and after the 1999 jökulhlaup were surveyed in 1996 and 2001 using photogrammetry (Staines et al., 2014). These datasets are a very unusual asset for this kind of modelling study. Although there are some slight changes within the river channel between the survey year and the jökulhlaup time, it was considered preferable to use the bed before the jökulhlaup rather than a post-flood bed as is often the case in jökulhlaup reconstructions (Staines, 2012). Thus, the 1996 digital elevation model (DEM) was used as the initial input domain for simulation, and the 2001 DEM was compared to the simulated bed. DEMs errors and uncertainty were assessed by comparing grid values with the differential Global Positioning System (dGPS) and with a DEM constructed from a 2010 summer LiDAR survey, which is assumed had no errors. More details about the surveyed dataset were given by Staines et al. (2014). In this study, the DEMs with two different resolutions (8 m × 8 m and 4 m × 4 m) were applied in order to elucidate the appropriate balance of computational efficiency and accuracy of the model.

Field observations indicate that the western conduit and the central conduit are two major sources from which floodwater flowed to the river channel. The observations with a peak discharge of 1700 m^3/s were made at the bridge after ~1 hour initiation of the 1999 jökulhlaup by Sigurdsson et al. (2000). The peak discharge was reconstructed to be 4000 m^3/s by Russell et al. (2010). Staines (2012) pointed out that the peak value 4000 m^3/s was rather high and defined a hydrograph with 40% of the discharge from the central conduit and 60% from the western conduit (Fig. 2) which was a good-fit to the observations. Thus, this study used the input hydrograph provided by Staines (2012) as the model input hydrograph.

Based on the field observations, the sediment material in the channel is constituted of various grain-sizes from fine granule to coarse boulder (Russell et al., 2010; Staines et al., 2014). The size fractions are summarised in Table 2 and include boulders, cobbles and granules. The median diameters for the three fractions differ significantly, and the distribution in reality is generally spatially varying. Grain-size is considered to be an uncertainty factor for morphodynamic modelling due to the difficulty in estimating the grain-size in a full-scale channel, and there are no proposed sediment transport equations for the transport of such coarse boulders. Also, the proportion of coarse boulders is small. Consequently, an appropriate simplification is made that only the sediment fractions of granules and cobbles were considered in the morphodynamic modelling. The proportion of both fractions was initially given as 50%. The updating of the proportion of each grain-size at each grid cell was calculated using the method described in section 2.5. To explore and emphasize the importance of grain-size on modelling results, we also used a single size fraction (d = 40 mm and d = 80 mm) for two runs.

Many studies have reported that Manning's roughness has significant effects on the modelled bed morphology, flow discharge and timing (Huang et al., 2014; Nicholas, 2003; Staines and Carrivick, 2015). Some studies used a constant Manning's value varying from 0.04 to 0.06 in proglacial areas comprising sand to cobble sized materials (Alho et al., 2005; Staines and Carrivick, 2015). To estimate the Manning's value, this study used the Manning-Strickler equation $n = 0.038d_{90}^{1/6}$ which is used to reconstruct the hydrograph of the 1999 jökulhlaup in the study area by Russell et al. (2010).

3. Hydro-morphodynamic model

3.1. Conceptual model structure

This study uses a layer-based conceptual model. The model which includes bedload has been developed and validated by Guan et al. (2014). As field evidence shows, the riverbed in the study site is composed of grains with a wide range from fine granules to coarse boulder. The jökulhlaup can not only induce the coarse particles in motion (bedload), but also entrains plenty of fine sediment particles in suspension because of the high bed shear stress. Therefore, the bedload dominant sheet flow model might be limited in simulating the whole range of geomorphological processes within the jökulhlaup. A suspended load model is crucial to reconstruct the physical processes more appropriately. In this regard, the model used in this study extended the layer-based bedload dominant sheet flow model by including an additional suspension layer. The model is a two-dimensional numerical model based on full shallow water equations for unsteady incompressible flow conditions. The main advantages of the model are that it calculates the natural velocity difference between the sheet flow layer and the mixed flow, and simulates the bank erosion as well. The depth-averaged 2D model was preferred because it has a higher computational efficiency over 3D modelling, and horizontal flow conditions were expected to predominate over vertical flows.

3.2. Hydrodynamic model

The 2D shallow water equations are solved using a Godunov-based finite volume method as in many existing flood models (Begnudelli and Sanders, 2006; Guan et al., 2013; Villanueva and Wright, 2006). The governing equations are extended with the incorporation of sediment transport and also considering the mass and momentum exchange of flow and bed. Based on the morphodynamic model proposed in previous work (Guan et al., 2014), the mass and momentum equations with sediment effects are written in vector form as follows:

$$\frac{\partial \mathbf{U}}{\partial t} + \nabla \cdot \mathbf{F} = \mathbf{S} \tag{1}$$

where **U** is the vector of conserved variables, **F** is the flux vector function and **S** is the vector of source terms, and $\nabla = \vec{\imath}(\partial/\partial x) + \vec{\jmath}(\partial/\partial y)$ is the gradient operator. **U**, **F** and **S** are

$$\mathbf{U} = \begin{bmatrix} \eta \\ hu \\ hv \end{bmatrix}, \quad \mathbf{F} = \begin{bmatrix} h\mathbf{V} \\ hu\mathbf{V} + \frac{1}{2}gh^2\vec{\imath} \\ hv\mathbf{V} + \frac{1}{2}gh^2\vec{\jmath} \end{bmatrix} \tag{2}$$

$$\mathbf{S} = \begin{bmatrix} 0 \\ gh\left(-\frac{\partial z_b}{\partial x} - S_{fx}\right) + \frac{\Delta\rho u}{\rho}\frac{\partial z_b}{\partial t}(\alpha(1-p) - C) - \frac{\Delta\rho g h^2}{2\rho}\frac{\partial C}{\partial x} - \mathbf{S_{ad}} \\ gh\left(-\frac{\partial z_b}{\partial y} - S_{fy}\right) + \frac{\Delta\rho v}{\rho}\frac{\partial z_b}{\partial t}(\alpha(1-p) - C) - \frac{\Delta\rho g h^2}{2\rho}\frac{\partial C}{\partial y} - \mathbf{S_{ad}} \end{bmatrix} \tag{3}$$

where h = flow depth (m); z_b = bed elevation (m); η = water surface (m); u, v = the x and y components of flow velocity respectively (m/s); **V** is the velocity vector defined by $\mathbf{V} = u\vec{\imath} + v\vec{\jmath}$; p = sediment porosity (dimensionless); C = total volumetric concentration (dimensionless); ρ_s, ρ_w = densities of sediment and water respectively (m^3/s); $\Delta\rho = \rho_s - \rho_w$; ρ = density of flow-sediment mixture (m^3/s); S_{fx}, S_{fy} are frictional slopes based on Manning's coefficient in x and y direction (dimensionless); $\alpha = u_s/u$ = sediment-to-flow velocity ratio (dimensionless) which represents the velocity difference of lower bedload transport and the mixed flow, the relationship defined by Greimann et al. (2008) was used as shown in Eq.(4); $\mathbf{S_{ad}}$ is the additional term vector related to the velocity ratio α defined by Eq.(5).

$$\alpha = \frac{u_*}{u}\frac{1.1(\theta/\theta_{cr})^{0.17}[1-\exp(-5\theta/\theta_{cr})]}{\sqrt{\theta_{cr}}} \tag{4}$$

$$\mathbf{S_{ad}} = S_A\vec{\imath} + S_B\vec{\jmath} = \frac{\Delta\rho\mathbf{V}}{\rho}(1-\alpha)[C\nabla\cdot(h\mathbf{V}) - (h\mathbf{V})\nabla\cdot\mathbf{C}] \tag{5}$$

where θ, θ_{cr} represent the real dimensionless bed shear stress, and the critical Shields parameter; **C** is the sediment concentration vector defined by $\mathbf{C} = C(\vec{\imath} + \vec{\jmath})$.

3.3. Sediment transport model

3.3.1. Sheet flow load

Sheet flow is conventionally referred to as bed-load transport occurring at high bottom shear stress. Sheet flow load generally has highly concentrated sediment in a layer near the bed with a thickness of several times the sediment grain size. The velocity in this layer is usually lower than the main water velocity (Pugh and Wilson, 1999; Sumer et al., 1996). To account this, a velocity difference coefficient α is included in this study. The mass conservation equation of the ith size class in sheet flow layer is written considering the velocity ratio α by the following equation (Guan et al., 2014).

$$\frac{\partial hS_{bi}}{\partial t} + \alpha\frac{\partial huS_{bi}}{\partial x} + \alpha\frac{\partial hvS_{bi}}{\partial y} = -\frac{\alpha(q_{bi} - F_i q_{b*i})}{L_i} \tag{6}$$

where S_{bi}=volumetric bedload concentration of the ith size class; q_{bi} = real sediment transport rate of the ith fraction; q_{b*i} = sediment transport capacity of the ith fraction; L_i = non-equilibrium adaptation length of sediment transport of the ith fraction, F_i represents the proportion of i th grain-size fraction in the total moving sediment.

Although there are a number of bedload transport formulae which were empirically proposed based on laboratory or fieldwork datasets, none can be universally applied to complex natural rivers due to the range and varying distribution of grain sizes. As suggested by Guan et al. (2014), this study chooses the combination of the modified Meyer-Peter & Müller formula (MPM) (Meyer-Peter and Müller, 1948) and the Smart & Jäggi formula (SJ) (Smart and Jäggi, 1983) based on the bed slopes. As the accuracy of the formulae has been considered to be poor, several other commonly-used formulae in the literature were also selected to conduct a sensitivity test. The bedload transport rate is written by:

$$q_{b*i} = \varphi\sqrt{g(\rho_s/\rho_w - 1)d_i^3} \tag{7}$$

where φ is determined by the following five selected formulae:

- A combination of MPM and SJ:

$$\varphi = \begin{cases} \psi 8\left(\theta_i - \theta_{cr,i}\right)^{1.5} & 0 \le S_o < 0.03 \\ 4\left(\frac{d_{90}}{d_{30}}\right)^{0.2} \frac{h^{1/6}}{n\sqrt{g}} \min(S_o, 0.2)\theta_i^{0.5}\left(\theta_i - \theta_{cr,i}\right) & S_o \ge 0.03 \end{cases}$$

- $\varphi = 8(\theta_i - \theta_{cr,i})^{1.5}$ for MPM
- $\varphi = 12{\theta_i}^{1.5}\exp\left(-4.5\theta_{cr,i}/\theta_i\right)$ for C&L (Camenen and Larson, 2005)
- $\varphi = 13{\theta_i}^{1.5}\exp\left(-0.05/{\theta_i}^{1.5}\right)$ for C (Cheng, 2002) :
- $\varphi = 12{\theta_i}^{0.5}\left(\theta_i - \theta_{cr,,i}\right)$ for N (Nielsen, 1992):

where S_o is bed slope; θ_{cri} is critical dimensionless bed shear stress of i th fraction; θ_i is the dimensionless bed shear stress of i th fraction. The non-equilibrium adaptation length is calculated by

$$L_i = \frac{h\sqrt{u^2 + v^2}}{\gamma\omega_{fi}} \text{ with } \gamma = \min\left(\alpha\frac{h}{h_b}, \frac{1-p}{C}\right) \tag{8}$$

in which, h_b is the thickness of sheet flow layer; ω_f is the effective setting velocity of sediment particle which is estimated using the formulation with hindered settling effect proposed by Soulsby (1997).

3.3.2. Suspended load transport

The advection-diffusion equation has been widely used for suspended load models (Carrivick et al., 2010; Wu, 2004; Yang et al., 2015) because of its accuracy in calculating the propagation of sediment concentration in a water body. This study utilised the depth-averaged 2D advection-diffusion equation for suspended transport as:

$$\frac{\partial hS_i}{\partial t} + \frac{\partial huS_i}{\partial x} + \frac{\partial hvS_i}{\partial y} = \frac{\partial}{\partial x}\left(\varepsilon_x h \frac{\partial S_i}{\partial x}\right) + \frac{\partial}{\partial y}\left(\varepsilon_y h \frac{\partial S_i}{\partial y}\right) + S_{E,i} - S_{D,i} \quad (9)$$

where S_i = volumetric suspended load concentration of the ith size class; $S_{E,i}$ = entrainment flux of sediment of the ith size class; $S_{D,i}$ = deposition flux of sediment of the ith size class; ε_x, ε_y = turbulent diffusion coefficients of sediment in the x and y direction. The first and second terms on the right hand side of Eq.(9) represent diffusion terms. Bohorquez and Ancey (2015) reported that sediment diffusion can induce bed instabilities and thereby provoke bed formation.

In Eq.(9), the entrainment flux and deposition flux for sediments are two vital parameters for updating the bed elevation, because both factors directly determine how much sediment is entrained and how much is deposited. However, a complete theoretical expression does not exist for the fluxes. In this study, a widely used approach is adopted (Wu et al., 2004).

$$S_{D,i} = \omega_{f,i} S_{a,i}, S_{E,i} = F_i \omega_{f,i} S_{ae,i} \quad (10)$$

where $S_{a,i}=\delta\ S_i$ is the near-bed concentration at the reference level a which refers to the depth of the sheet flow layer; the definition of the coefficient δ by Cao et al. (2004) is used as $\delta = \min\{2.0, (1-p)/C\}$; $S_{ae,i}$ is the near bed equilibrium concentration at the reference level determined by the empirical equation of van Rijn (1984); the fraction coefficient F_i is defined in section 3.5. The deposition flux is represented as a product of the effective sediment settling velocity and the near-bed concentration at the reference level. The near bed equilibrium concentration is given as:

$$S_{ae,i} = 0.015 \frac{d_i}{a} \frac{T_i^{1.5}}{d_{*i}^{0.3}} \quad (11)$$

$$T_i = \frac{(u_{*i}^2 - u_{*i,cr}^2)}{u_{*i,cr}^2};\ a = \min[\max(\mu\theta_i d_{50}; 2d_{50}; 0.01h), 0.2h]$$

where T_i is the transport stage parameter; $u_{*i} = (g^{0.5}/C')u$ is bed-shear velocity related to grains; C' is the Chézy-coefficient related to grain; $u_{*i,cr}$ is the critical bed-shear velocity.

3.4. Morphological evolution model

Erosion and deposition is calculated per grid cell at each time step to update the new bed elevation on the basis of the results from the hydrodynamic model and sediment transport model described above. The morphological evolution for non-uniform sediment material is calculated by:

$$\frac{\partial z_b}{\partial t} = \frac{1}{1-p}\sum_{i=1}^{N}\left[\frac{(q_{bi} - F_i q_{b*i})}{L_i} + S_{D,i} - S_{E,i}\right] \tag{12}$$

where the parameters on the right side are calculated according to the equations in previous sections.

3.5. Model consideration

The above coefficient F_i represents the proportion of i th grain-size fraction in the total sediment in motion. It varies with time so F_i is updated at each time step. The updating of bed material composition is an essential process for non-uniform bed aggradation and degradation. Among the three classified layers in the model, it is the active layer that participates in the exchange with moving sediment. There are several bed material sorting models available in the literature; the approach presented by Wu (2004) is adopted in this study. The method divides the bed material above the non-erodible bed into several layers. The top layer is the mixed layer where the exchange with the moving sediment occurs. The variation of bed material gradation in the mixed layer is then updated at each time step.

Since the grain-size in the study domain varies greatly, the hiding/exposure effects between particles and particles are important for the incipient motion and settling of sediments. Thus, this study accounts for such effects in the estimation of the threshold for sediment incipient motion. Flood-induced erosion within the main channel can cause further bank erosion. Also, the simulated morphological evolution can generate an over-steep bed which is naturally unstable. To address this, this study utilised a bank failure model developed by Guan et al. (2014) to update the unstable newly deformed bed. The model uses different critical bed angles and re-formation bed angles above and below the water. Both the calculation of sediment incipient motion and the bank failure model are given in details by Guan et al. (2014) and so for brevity are not repeated here.

The 2D hydro-morphodynamic model system consists of Eq.(1), Eq.(6), Eq.(9) and Eq.(12). In this study, a second-order Godunov-type finite volume method (Guan et al., 2014) is used to solve the improved hydro-morphodynamic model considering both bedload and suspended load. A variable time step Δt, adapted to local flow conditions, is calculated at each time step by the following equation.

$$\Delta t = CFL \min\left(\min \frac{dx_i}{|u_i|+\sqrt{gh_i}}, \min \frac{dy_j}{|v_j|+\sqrt{gh_j}}\right) \quad (13)$$

As the numerical scheme is explicit, the restriction of Courant number $0<CFL<1.0$ is implemented for the calculation of flow sediment transport, and bed change. The inclusion of sediment transport model requires the reduction of the CFL number to maintain the model stability, which increases the computational time.

4. Results and discussion

4.1. Sensitivity of grain size

Table 3 shows the simulated extent of bed erosion and deposition for the three scenarios with different grain-size inputs. It indicates that the total bed change area is 2.51 km^2 for the mixed grain-size (the mixture of granules and cobbles shown in Table 2) which is larger than the bed change area of 2.08 km^2 for d = 40 mm whilst the extent of bed change for d = 80 mm is the smallest for the three cases, at only 1.60 km^2. Fig. 3 demonstrates the spatial distribution of the simulated bed erosion and deposition in the river channel. It is clearly shown that the extent of bed change for d = 80 mm is much smaller than that for the other two. The extent of bed change for the mixed grain-size input is the broadest in the three cases. Although the maximum depth of erosion and deposition do not differ from each other greatly, the simulation with mixed grain-size predicts more erosion and deposition within the channel than other scenarios. For example, in the highlighted circular area of Fig. 4, erosion and deposition hardly occur for the scenario with d = 80mm, yet, we found significant erosion and deposition with the input of mixed grain-size. There are a couple of reasons causing these differences. First, a different grain-size estimates a different Manning's roughness which affects the calculation of bed shear stress. A more important reason is that finer sediment particles have a smaller settling velocity, and higher dimensionless bed shear stress induces the finer particles into motion more easily, even with relative weak flows. The results imply that for a real flood over non-uniform bed, the use of a single grain-size might cause over-/under-prediction of morphological changes. It is necessary to adopt the appropriate representative fractions of grain-size which can reflect the natural conditions as realistically as possible.

4.2. Sensitivity of sediment transport functions

Fig. 4 plots the simulated temporal change of bed erosion and deposition volumes during the flood as modelled with different transport formulae. Fig. 4a indicates that the overall trends for the five runs are similar, with all increasing rapidly before the peak stage of t = 2 hours and then reaching an approximately constant value. However, the deposition volumes differ from each other. The difference of 0.67×10^5 m^3 is 12.1%. The plot of the erosion volumes shows more significant differences with a maximum of 1.61×10^5 m^3, i.e. about 21%. The bed changes simulated by the formulas of MPM and C&L differ slightly from each other. The formulas of C, N and MPM&SJ led to more severe erosion and deposition than MPM and C. Fig. 4b shows the total area of simulated net sediment erosion and aggradation. It is noted in Fig. 4b that both erosion area and deposition area are influenced only slightly by the sediment transport formulae. The areal extents of the total bed changes for the five runs are also found to be similar with a difference smaller than 1%. The sensitivity test in this section reveals that the empirical transport functions can affect the magnitude of net bed erosion and deposition, but qualitatively, the sensitivity of bed change features to these functions is slight. It should be noted that the sensitivity test is to explore the effects of different existing empirical bedload functions on simulated results, it does not account for the uncertainty factors such as the critical Shields number, the probability of sediment entrainment as bedload and suspended load, and particle diffusivity etc. The slight sensitivity verified here does not imply that the simulation results by the model is as accurate as the real field observation, but means that the model is significantly affected by the choice of empirical transport functions.

4.3. Implications of DEM resolution

Higher resolution topographic data can represent geomorphology more accurately, but at the expense of increasing simulation time. To examine the appropriate balance between these two factors, bed topography at two resolutions (Run 1: 8 m×8 m and Run 2: 4 m×4 m) was tested in this study. Table 4 indicates that the simulated total erosion and deposition volumes are 7.8×10^5 m^3 and 5.9×10^5 m^3 respectively for Run 2, while for Run 1, the total erosion and deposition are 7.4×10^5 m^3 and 5.5×10^5 m^3, respectively. The differences for erosion and deposition are 0.4×10^5 m^3 (4.4%) and 0.4×10^5 m^3 (5.8%), respectively. At the cross section x = 332908.86 m close to a bridge which is located in the middle of the channel, it is found that the difference of the maximum water level is just 0.08 m. Furthermore, the simulated temporal evolution of both erosion and deposition volumes have a similar trend of increase and then tend to a constant value. Both total erosion and deposition volumes are very close before 1.5 hours; but at later times, both are slightly larger for Run 2 than those for the Run 1. Fig. 5 (a, b) demonstrates that the spatial pattern and extent of the erosion and deposition for the two runs are in general similar, and both runs predict the maximum erosion and deposition depths with a slight difference. Fig. 5(c) shows that the difference of Run 2 and Run 1 occurs across the whole channel. However, we found both mean +/- differences are smaller than 0.2 m. The results indicate that the DEM resolution slightly affects the simulated spatial distribution of bed changes. This is because the finer resolution DEM represents the bed terrain with more detail, thus the simulated flow conditions (velocity and water depth) will be slightly different. However, the computational time for the finer resolution is higher by a factor of over four than that for the coarser one.

In summary, whilst topography is very important for defining the transient nature of outburst flood hydraulics and geomorphological change (e.g.(Carrivick et al., 2013b)), the implications of varying input topography resolutions in this study shows that: (1) the simulated net bed erosion and deposition for the finer 4 m × 4 m resolution is slightly more severe than those for the coarser 8 m×8 m DEM; (2) both the simulated bed change have a similar pattern and extent; however, (3) the computational time for the finer 4 m×4 m DEM is four times more expensive than that for the coarser 8 m × 8 m resolution; (4) so the coarse resolution of 8 m×8 m is sufficient for the geomorphological analysis herein.

4.4. Multiple effects of sediment transport

Sediment transport entrained by outburst floods has the potential to affect the flow hydraulics by modifying the flow density, the flow viscosity and the turbulence regime. Hence, the frontal wave speed, the flow velocity as well as the flow depth will be altered considerably due to the incorporation of sediment transport in flood propagation (Carrivick et al., 2011; Fraccarollo and Capart, 2002; Zech et al., 2008). In this section, the effects of sediment transport on flood propagation are discussed and analysed from the numerical modelling of a large-scale (field) event. In order to achieve this, two scenarios are modelled, namely: a clear water flood without sediment transport (denoted Run 1); and a water-sediment mixed flood with sediment transport (denoted Run 2). The two scenarios are compared via flow discharge at the cross section (x=332908.86) near the bridge and the water surface at a gauge (332908.86, 480099.78), as shown in Fig. 6. It reveals the following key points.

- The peak flow discharge at the cross section x = 332908.86 m increases slightly by 22 m^3/s (1%) from 2111.5 m^3/s to 2133.5 m^3/s. Also during the flood period, the volume of the sediment-laden flow through the cross section is about 2.09×10^7 m^3, while the fluid volume is approximately 2.02×10^7 m^3. The incorporation of sediment transport leads the flow volume to increase by 7.0×10^5 m^3. This manifests the bulk effects of sediment entrainment within sediment-laden floods. During the outburst flood, the total erosion volume is about 7.4×10^5 m^3, and the deposition volume is 5.5×10^5 m^3, i.e. a net riverbed change with a volume of 1.9×10^5 m^3 occurs during the whole flood period. The modelled net loss clarifies the source of the increased flow volume within the sediment-laden flood.
- The water level with sediment at the point (332908.86, 480099.78) is smaller than that without sediment throughout the flood period apart from a short initial stage, because the sediment-laden flow arrives at the location earlier than the clear water flood. The decrease of water level in the falling period is particularly significant.
- The water depth against time at the gauge point is also changed greatly due to the inclusion of in-channel erosion and deposition. Specifically, the maximum water depth with consideration of sediment transport is approximately 3.45 m, 0.47 m larger than that without sediment transport of

2.98 m. The water depth becomes smaller after the peak flow discharge as a result of the bed deformation caused by the flood;

- As expected, the arrival time of the peak discharge at the cross section for Run 2 is considerably shorter than that for Run 1 (Table 5), the time difference is 7.2 minutes. The arrival time of the water front is also decreased by about 2.6 minutes due to the incorporation of sediment transport. The faster propagation of waterfront and peak flows of the flood has also been found by Staines and Carrivick (2015), who conclude that a morphodynamic model advanced flood arrival and peak discharge times by 100% and 19% over hydrodynamic model. The simulated arrival time of peak flow to the bridge is about 1 hour 13 minutes, which overall agrees with the recorded time by Sigurdsson et al. (2000) and with the investigation by (Staines, 2012).

In summary, the outburst flood changes the bed terrain, which alters the flood dynamics, such as the water level, the water depth and the flow velocity field etc. Fig. 7 shows that: the differences of the minimum bed elevation have positive values and negative values (63.3% and 36.7% respectively) because of the erosion and deposition caused by the jökulhlaup; the maximum water surface and maximum water depth for Run 2 are significantly smaller than those for Run 1 at most cross sections (89.8% and 86.1% respectively). Table 6 shows the statistics of the simulated results for the two runs. The water levels are reduced due to inclusion of sediment transport in an area of approximately 3.03 km^2, whilst the water levels are raised in an area of only 0.76 km^2. The water depths decrease and increase in an area of approximately 2.68 km^2 and 1.11 km^2, respectively. In addition, the flood submerged area simulated by Run 1 is about 0.34 km^2 larger than the submerged area for Run 2.

Fig. 8 illustrates the flow velocity fields of the two runs at the peak stage of t=2 hours. In overview both flow fields show similar patterns in terms of the regions of high velocity and low value, yet the absolute magnitudes appear to be different. Specifically, the surface of flow velocity field shows a smooth contour distribution for the sediment-laden flood, whereas some fluctuations occur in the surface of the contour distribution for the clear water flood. This characteristic is also shown in the spatial distribution of the water depth in the river channel. Clearly, the changes in flood dynamics are caused by in-channel erosion and deposition due to the rapid flood. It is inferred that the flood water induces sediment transport, creating a smoother topography and thereby improves the flow conveyance capacity of the river channel, which in return enables the flood to propagate faster. Incorporation of sediment transport promotes a faster (shorter) arrival time of the water front and the peak flow discharge.

4.5. Erosion and deposition

The 1999 jökulhlaup eroded and carried a considerable amount of sediment, causing rapid bed change (e.g. Russell et al. 2013). However, it is quite challenging to quantify the volume and the rate of bed erosion and deposition at both temporal-scale and spatial-scale by physical measurements in the field (Russell et al. 2013). Therefore this study presents further understanding of these processes that can be derived from the applications of a morphodynamic model. To verify the capability of the model in predicting geomorphological changes, the difference of DEMs (DoD) before (1996 DEM) and after (2001 DEM) the 1999 jökulhlaup was used to compare to the simulated riverbed changes, which is demonstrated in Fig.9. It indicates that the simulated spatial pattern of bed erosion and deposition is in general agreement with the difference of DEMs before and after the flood. For example, in the highlighted circle zones of Fig.9 (a,b), the location and magnitude of bed changes are properly simulated, which agrees with the measurement fairly well and is not just limited to the circular areas but in other regions of the channel, where and how river morphology changes are reasonably predicted. Inevitably, there are some discrepancies between the measured and the modelled in terms of the depth in erosion and deposition. The measurements show that the riverbed is changed in a wider area. The difference between the DoD and the modelled results is demonstrated in Fig.9 (c). The mean difference between the two is in the range of (-0.78m – 0.92m), which means only two-boulder diameters (diameter of a boulder is 0.4 m). The difference in the volume and depth of bed changes is attributed to several uncertainty factors as investigated by Staines (2012). First, the time scale between the measurement and the simulation is different; the time interval between the two DEMs before and after the flood is ~ 5 years, yet the simulation time is only 6 hours for the flooding period. There must be geomorphological activity during the 5 years which is one of the uncertainties in this study. Second, the jökulhlaup can carry a large amount of sediment materials from upstream glacial areas, but it is difficult to quantify the accurate volume. Furthermore, the empirical parameterisation for model input may influence the simulated results, such as the Manning's value, the empirical transport rates, entrainment and deposition fluxes. Fig. 10 plots the comparison at four cross sections to further demonstrate the agreement and difference between the measurement and the simulation. It can be seen that the modelled bed agrees with the surveyed bed after the flood very well at CS1 and CS3, while significant differences are found at some parts of CS2 and CS4. As discussed before, the difference is caused by the uncertainties in the model and its parameters. Overall, the present model is capable of predicting reasonably where and how the river geomorphology changes during the 1999 jökulhlaup, which gives confidence for further assessment of the geomorphological behaviours within the flooding.

From the final spatial pattern of net bed change, it is seen that the modelled outburst flood causes erosion and deposition to occur in the main channel, and both are more severe in the narrower reach of the river, because the water depth and flow velocity are higher in the narrower channel, increasing the bed shear stress, which induces more sediments into motion. To further demonstrate flood-induced scour, Fig. 11 plots the bed topography of a reach near the bridge before the flood, at the peak stage and after the flood. The changes during the three stages clearly demonstrate that the main channel is expanded due to erosion. The temporal evolution of the total erosion and deposition volume, as well as the net erosion are shown in Fig. 12. Points of note, are that:

(1) the total erosion volume accumulates and increases rapidly in the rising phase of the flow discharge as a result of the more intense bed shear stress, and the entrained sediment load in the water body then re-deposits within a certain transport distance;

(2) during the peak flow stage, the total erosion and deposition volumes increase continually, and after 2.5 hours, both tend to reach an approximate constant value;

(3) the volume of net change (erosion minus deposition) steadily increases with the inundation time, i.e. increasingly more sediment is entrained into the water body, which must increase the total fluid volume; this outcome implies the bulk effects of sediment entrainment as shown in Section 4.4 above; (4) in the flood recession limb, bed changes are weakened with slightly bedform development.

In this jökulhlaup, the final deposition volume is modelled to be approximately 5.5×10^5 m^3 and the total erosion volume to be about 7.4×10^5 m^3. The net riverbed change is 1.9×10^5 m^3, which indicates how much sediment was transported into the downstream sea along with the jökulhlaup. The majority of the bed erosion and deposition occurs within approximately 2-3 hours of the flood initiation; conversely, bed scour rarely takes place in the recession limb of the flood. To demonstrate the sediment-laden flood inundation process, Fig. 13 illustrates the water depth and the resulting spatial pattern of bed changes at several indicative time steps. In summary, this sub-set of results indicates that:

- the outburst flood causes rapid geomorphological change; the bed degradation and aggradation mostly occur in the initial 2-3 hours when the flood is increasing,
- net erosion occurs within the flood, and erosion increases progressively with inundation time, and
- the narrower the initial channel is, the more severe the flood-induced bed erosion and deposition.

In order to show the changes of flow conveyance capacity due to bed erosion and deposition, Manning's equation is used to estimate the discharge capacity of an open channel following Pepper and Rickard (2009).

$$Q_c = \frac{AR^{2/3}\sqrt{i}}{n}$$

where: Q_c = discharge capacity (m^3/s); A = area of cross section of flow (m^2); R = A/P = the hydraulic radius, (m); P = wetted perimeter of the channel cross section (m); i = hydraulic gradient (usually approximated by the longitudinal slope of the channel). The term, $\sqrt{i}/n$, could be approximately considered to be unchanged before and after the flood. Thus, the changes of the flow conveyance capacity can be approximately taken as A and P. At a single cross section, net erosion can lead to a significant increase of A, but the wetted perimeter P is only slightly affected, resulting in an increase in $AR^{2/3}$. Net erosion increases with the inundation time (Fig. 11). The final net eroded volume reaches 1.9×10^5 m^3. This outcome implies that the flow conveyance capacity of the river channel will be raised with the net increase of erosion in the channel, which also gives a reason why the flood propagation is accelerated by the inclusion of sediment transport during the outburst flood.

4.6. Wider discussion

Here we suggest that whilst the exact prediction of bed change is still unattainable, the application of numerical models can enhance and improve insights into real-world outburst floods via both quantitative analysis and qualitative assessment of the model outputs. Additionally, since any model output admittedly has uncertainties, this study has sought to determine the sensitivity of a model to representations of the major morphodynamic processes.

The previous theoretical, small-scale numerical and experimental studies (Bohorquez and Ancey, 2015; Cao et al., 2004; Carrivick et al., 2011) have provided fundamental insight on the complex interaction between outburst flows and a movable bed. However, these studies have unknown representation of geomorphological processes within large-scale (field) outburst floods, because amongst other properties the real-world topography is generally complex, the real-world grain size distribution is spatial varying, and the real-world erosion and deposition in outburst floods occurs vertically and laterally. From a spatial-scale application, this study found that the effects of sediment transport on flood dynamics were significant and must be treated within outburst flood modelling (Fig. 6-Fig. 8). These findings agree with recent studies that have also investigated the effects of morphological change on flood dynamics at large-scale, e.g. (Bohorquez and Darby, 2008; Li et al., 2014; Wong et al., 2014). Wong et al. (2014) reported that the inclusion of bed elevation changes appeared to alter flood dynamics locally, but that it was not significant for flood inundation, so hydraulic models do not need to account for morphodynamic changes within events. However, their study only considered bed erosion, and neglected deposition, which according to the findings of this study cause effects on flood hydraulics that are far greater than for erosion. Furthermore, this study has indicated that flow bulking effects due to sediment entrainment can influence flood propagation, and this is a property of outburst floods that is not explicitly considered in the study of Wong et al.(2014). Li et al. (2014) showed that very strong bed erosion and the decrease of bed friction due to bed change led to an increase of peak flow discharge within hyperconcentrated floods in the Yellow River. Yet, in the study by Li et al. (2014), the flood dynamics and geomorphological processes within floods were not identified. The results presented in this study demonstrate that both water surface and water depth at the peak stage were reduced in most areas of the river channel with consideration of morphological changes, the flood propagation was accelerated notably, peak flows in particular, and the water volume was increased because of sediment entrainment. The inundation extent was slightly affected by morphological changes for the specific case (Table 6) in general agreement with the finding by Wong et al. (2014). We also found that morphological changes caused river channel adjustment conducive to flood propagation (Fig. 12), which reflected the effects of sediment transport on flood dynamics. The fundamental reasons that sediment transport affects flood dynamics can be summarized as: (1) sediment entrainment into the floodwater and the rheology of sediments increase the density of the fluid flows, thereby increasing the flow mass and accelerating flood propagation; (2) the flood-induced net erosion enhanced the flow conveyance capacity of the river channel, which is elucidated above in Section 4.5. All these results greatly improved the understanding of the importance of geomorphological changes within inundation modelling.

In this study, the morphodynamic model has quantified the spatio-temporal bed degradation and aggradation, including spatial patterns, volumes and rates, caused by the 1999 jökulhlaup. Although there is a discrepancy between the modelled landscape changes and the DoD because of the uncertain sediment activity during the long-time interval (5 years) for measurements before and after the flood (Staines, 2012), the morphodynamic model predicted the landscape change pattern in general agreement with the measured pattern. This gives confidence in the assessment of geomorphological impacts during the 1999 jökulhlaup quantitatively and qualitatively via the morphodynamic model. Future studies can use the model presented herein to assess flood-induced geomorphological changes in the context of annual and seasonal intra-catchment sediment fluxes and geomorphological activity (e.g.(Carrivick et al., 2013a)). In the modelled jökulhlaup, the geomorphological changes were more severe when the flood was at the rising and peak stage. The temporal change of total erosion and deposition volume within the outburst flood increased rapidly on the rising limb and was slowed down in the flood recession. This relative timing of geomorphological work was also reported in the study of (Carrivick et al., 2010). Additionally, we found in this study that geomorphological adjustments by an outburst flood can modify bed friction which with the new topography can further alter the dynamics of subsequent floods in flood sequences. This has revealed the importance and necessity for river flood modelling to consider the associated geomorphological impacts. In summation, the prediction of both hydrodynamic and morphodynamic aspects of outburst floods can provide valuable information for flood risk assessment that hydrodynamic models run over a fixed bed cannot.

5. Conclusions

This study presented a 2D hydro-morphodynamic model designed for outburst floods which consider a bedload and suspended load, non-uniform sediment grain-size distribution effects, bed slope effects and different velocities for each vertical layer. A large-scale volcano-induced jökulhlaup has been reproduced by this model. Comparison with the surveyed landscape change has indicated that the model is capable of predicting geomorphological changes due to a jökulhlaup reasonably well. Based on the results and discussion presented above, the study improved understanding of geomorphological processes within the 1999 jökulhlaup and the effects of river channel changes on flood dynamics.

In this study of the Sólheimajökull flood, it has been calculated that a large amount of sediments of the order of 10^5 m^3 transport occurred during the jökulhlaup. The net change (minus) occurred during the whole flood period, and the net volume increased along with the flood (Fig. 12). It was also found that bed changes were more active in the rising limb during which over 75% bed changes were finished. The peak erosion rate and deposition rate occurred at the peak stage. In the falling limb, there was only slight bedform development, but both total erosion and deposition volume did not increase greatly (Fig. 12).

More widely, it has firstly been confirmed that grain-size significantly affects the geomorphological changes because of the resulting effects on Manning's roughness and bed shear stress. This suggests that a representative parameterisation of spatially varying grain-size is vital for morphodynamic modelling of real-life floods with geomorphological changes. For numerical modelling, although the accuracy of sediment transport formula is generally considered poor, the features of riverbed changes are not greatly influenced by the choice of formulae. The influence of DEM resolution is also insignificant in quantifying outburst flood dynamics and geomorphological changes.

Secondly, the analysis has verified that the net change (minus) during an outburst flood can lead to an increase of the flow conveyance capacity of the river channel, and the in-channel scour can reduce the Manning's value. This implies that flood propagation becomes 'smoother' or 'easier' due to rapid river channel adjustment. This is why the inclusion of sediment transport and geomorphological changes accelerate the inundation over the hydrodynamic modelling over fixed bed. Effects of geomorphological changes on flood dynamics are also apparent in water levels and water depths within the river channel that are mostly reduced for an event where net erosion occurs. Furthermore, the bulking effects of intense and voluminous sediment entrainment increase not only the flow volume, but also the downstream peak discharge, and the increase rate is dependent on how much sediment is entrained to floods. This effect of morphodynamics is very important because water levels, peak flow, and the time of flood are the generally preferred important indicators for flood risk assessment. Therefore, a major implication of this study is the verification of the significant impacts of geomorphological changes on hydraulics required for flood risk assessment during an event where erosion and deposition is severe.

References

Alho, P., Russell, A.J., Carrivick, J.L., Käyhkö, J., 2005. Reconstruction of the largest Holocene jökulhlaup within Jökulsá á Fjöllum, NE Iceland. Quaternary Science Reviews, 24(22): 2319-2334. DOI:10.1016/j.quascirev.2004.11.021

Begnudelli, L., Sanders, B.F., 2006. Unstructured grid finite-volume algorithm for shallow-water flow and scalar transport with wetting and drying. Journal of Hydraulic Engineering-ASCE, 132(4): 371-384. DOI:10.1061/(asce)0733-9429(2006)132:4(371)

Berzi, D., Jenkins, J.T., 2008. A theoretical analysis of free-surface flows of saturated granular–liquid mixtures. Journal of Fluid Mechanics, 608: 393-410. DOI:doi:10.1017/S0022112008002401

Bohorquez, P., Ancey, C., 2015. Stochastic-deterministic modeling of bed load transport in shallow water flow over erodible slope: Linear stability analysis and numerical simulation. Advances in Water Resources, 83(0): 36-54. DOI:http://dx.doi.org/10.1016/j.advwatres.2015.05.016

Bohorquez, P., Darby, S.E., 2008. The use of one- and two-dimensional hydraulic modelling to reconstruct a glacial outburst flood in a steep Alpine valley. Journal of Hydrology, 361(3–4): 240-261. DOI:http://dx.doi.org/10.1016/j.jhydrol.2008.07.043

Camenen, B., Larson, M., 2005. A general formula for non-cohesive bed load sediment transport. Estuarine, Coastal and Shelf Science, 63(1–2): 249-260. DOI:http://dx.doi.org/10.1016/j.ecss.2004.10.019

Cao, Z., Pender, G., Wallis, S., Carling, P., 2004. Computational dam-break hydraulics over erodible sediment bed. Journal of Hydraulic Engineering-ASCE, 130(7): 689-703. DOI:10.1061/(asce)0733-9429(2004)130:7(689)

Carling, P. et al., 2010. Unsteady 1D and 2D hydraulic models with ice dam break for Quaternary megaflood, Altai Mountains, southern Siberia. Global and Planetary Change, 70(1-4): 24-34. DOI:10.1016/j.gloplacha.2009.11.005

Carling, P.A., 2013. Freshwater megaflood sedimentation: What can we learn about generic processes? Earth-Science Reviews, 125(0): 87-113. DOI:http://dx.doi.org/10.1016/j.earscirev.2013.06.002

Carrivick, J.L. et al., 2013a. Contemporary geomorphological activity throughout the proglacial area of an alpine catchment. Geomorphology, 188(0): 83-95. DOI:http://dx.doi.org/10.1016/j.geomorph.2012.03.029

Carrivick, J.L., Jones, R., Keevil, G., 2011. Experimental insights on geomorphological processes within dam break outburst floods. Journal of Hydrology, 408(1–2): 153-163. DOI:10.1016/j.jhydrol.2011.07.037

Carrivick, J.L., Manville, V., Graettinger, A., Cronin, S.J., 2010. Coupled fluid dynamics-sediment transport modelling of a Crater Lake break-out lahar: Mt. Ruapehu, New Zealand. Journal of Hydrology, 388(3-4): 399-413. DOI:10.1016/j.jhydrol.2010.05.023

Carrivick, J.L., Rushmer, E.L., 2006. Understanding high-magnitude outburst floods. Geology Today, 22(2): 60-65. DOI:10.1111/j.1365-2451.2006.00554.x

Carrivick, J.L., Turner, A.G.D., Russell, A.J., Ingeman-Nielsen, T., Yde, J.C., 2013b. Outburst flood evolution at Russell Glacier, western Greenland: effects of a bedrock channel cascade with intermediary lakes. Quaternary Science Reviews, 67(0): 39-58. DOI:http://dx.doi.org/10.1016/j.quascirev.2013.01.023

Cheng, N., 2002. Exponential Formula for Bedload Transport. Journal of Hydraulic Engineering, 128(10): 942-946. DOI:doi:10.1061/(ASCE)0733-9429(2002)128:10(942)

Dai, F.C., Lee, C.F., Deng, J.H., Tham, L.G., 2005. The 1786 earthquake-triggered landslide dam and subsequent dam-break flood on the Dadu River, southwestern China. Geomorphology, 65(3-4): 205-221. DOI:10.1016/j.geomorph.2004.08.011

Fischer-Antze, T., Olsen, N.R.B., Gutknecht, D., 2008. Three-dimensional CFD modeling of morphological bed changes in the Danube River. Water Resources Research, 44(9): W09422. DOI:10.1029/2007WR006402

Fraccarollo, L., Capart, H., 2002. Riemann wave description of erosional dam-break flows. Journal of Fluid Mechanics, 461: 183-228. DOI:http://dx.doi.org/10.1017/S0022112002008455

Greimann, B., Lai, Y., Huang, J.C., 2008. Two-dimensional total sediment load model equations. Journal of Hydraulic Engineering-ASCE, 134(8): 1142-1146. DOI: http://dx.doi.org/10.1061/(ASCE)0733-9429(2008)134:8(1142)

Guan, M., Wright, N., Sleigh, P., 2013. A robust 2D shallow water model for solving flow over complex topography using homogenous flux method. International Journal for Numerical Methods in Fluids, 73(3): 225-249. DOI:10.1002/fld.3795

Guan, M., Wright, N., Sleigh, P., 2014. 2D Process based morphodynamic model for flooding by noncohesive dyke breach. Journal of Hydraulic Engineering, 140(7). DOI:10.1061/(ASCE)HY.1943-7900.0000861

Guan, M., Wright, N., Sleigh, P., 2015. Multimode morphodynamic model for sediment-laden flows and geomorphic impacts. Journal of Hydraulic Engineering. DOI:doi:10.1061/(ASCE)HY.1943-7900.0000997

Huang, W., Cao, Z.-x., Carling, P., Pender, G., 2014. Coupled 2D hydrodynamic and sediment transport modeling of megaflood due to glacier dam-break in Altai Mountains, Southern Siberia. J. Mt. Sci., 11(6): 1442-1453. DOI:10.1007/s11629-014-3032-2

Huggel, C., Kaab, A., Haeberli, W., Teysseire, P., Paul, F., 2002. Remote sensing based assessment of hazards from glacier lake outbursts: a case study in the Swiss Alps. Canadian Geotechnical Journal, 39(2): 316-330. DOI:10.1139/t01-099

Khosronejad, A., Rennie, C., Salehi Neyshabouri, S., Townsend, R., 2007. 3D Numerical modeling of flow and sediment transport in laboratory channel bends. Journal of Hydraulic Engineering, 133(10): 1123-1134. DOI:doi:10.1061/(ASCE)0733-9429(2007)133:10(1123)

Li, W., van Maren, D.S., Wang, Z.B., de Vriend, H.J., Wu, B., 2014. Peak discharge increase in hyperconcentrated floods. Advances in Water Resources, 67(0): 65-77. DOI:http://dx.doi.org/10.1016/j.advwatres.2014.02.007

Manville, V., White, J.D.L., Houghton, B.F., Wilson, C.J.N., 1999. Paleohydrology and sedimentology of a post-1.8 ka breakout flood from intracaldera Lake Taupo, North Island, New Zealand. Geological Society of America Bulletin, 111(10): 1435-1447. DOI:10.1130/0016-7606(1999)111<1435:pasoap>2.3.co;2

Meyer-Peter, E., Müller, R., 1948. Formulas for bed load transport, Stockholm, Sweden.

Nicholas, A.P., 2003. Investigation of spatially distributed braided river flows using a two-dimensional hydraulic model. Earth Surface Processes and Landforms, 28(6): 655-674. DOI:10.1002/esp.491

Nielsen, P., 1992. Coastal bottom boundary layers and sediment transport. Advanced Series on Ocean Engineering, 4. World Scientific, 324 pp.

Pepper, A., Rickard, C., 2009. Works in the river channel. In: Ackers, J.C., Rickard, C.E., Gill, D.S. (Eds.), Fluvial Design Guide. Environment Agency, pp. 8.1-8.36.

Pugh, F.J., Wilson, K.C., 1999. Velocity and concentration distributions in sheet flow above plane beds. Journal of Hydraulic Engineering-ASCE, 125(2): 117-125. DOI:10.1061/(asce)0733-9429(1999)125:2(117)

Roberts, M.J., Tweed, F.S., Russell, A.J., Knudsen, Ó., Harris, T.D., 2003. Hydrologic and geomorphic effects of temporary ice-dammed lake formation during jökulhlaups. Earth Surface Processes and Landforms, 28(7): 723-737. DOI:10.1002/esp.476

Russell, A.J., Tweed, F.S., Knudsen, Ó., 2000. Flash flood at Sólheimajökull heralds the reawakening of an Icelandic subglacial volcano. Geology Today, 16(3): 102-106. DOI:10.1046/j.1365-2451.2000.00005.x

Russell, A.J. et al., 2010. An unusual jökulhlaup resulting from subglacial volcanism, Sólheimajökull, Iceland. Quaternary Science Reviews, 29(11–12): 1363-1381. DOI:http://dx.doi.org/10.1016/j.quascirev.2010.02.023

Shimizu, Y., Yamaguchi, H., Itakura, T., 1990. Three-dimensional computation of flow and bed deformation. Journal of Hydraulic Engineering, 116(9): 1090-1108. DOI:doi:10.1061/(ASCE)0733-9429(1990)116:9(1090)

Sigurdsson, O., Zóphóníasson, S., Ísleifsson, E., 2000. Jökulhlaup úr Sólheimajökull 18, júlí 1999. , 49, . Jökull, 49: 75-81.

Smart, G., Jäggi, M., 1983. Sediment transport on steep slopes. Mitteilung. 64. Versuchsanstalt fu¨ r Wasserbau, Hydrologie und Glaziologie, ETH Zurich, Zurich.

Soulsby, R., 1997. Dynamics of marine sands: a manual for practical applications. Thomas Telford, London, UK, 249 pp.

Staines, K.E.H., 2012. Quantifying Landscape Change in a Jökulhlaup-prone Proglacial System Sólheimajökull, Southern Iceland, University of Leeds, Leeds, UK, 224 pp.

Staines, K.E.H., Carrivick, J.L., 2015. Geomorphological impact and morphodynamic effects on flow conveyance of the 1999 jökulhlaup at sólheimajökull, Iceland. Earth Surface Processes and Landforms: n/a-n/a. DOI:10.1002/esp.3750

Staines, K.E.H. et al., 2014. A multi-dimensional analysis of pro-glacial landscape change at Sólheimajökull, southern Iceland. Earth Surface Processes and Landforms: n/a-n/a. DOI:10.1002/esp.3662

Sumer, B.M., Kozakiewicz, A., Fredsoe, J., Deigaard, R., 1996. Velocity and concentration profiles in sheet-flow layer of movable bed. Journal of Hydraulic Engineering-ASCE, 122(10): 549-558. DOI:http://dx.doi.org/10.1061/(ASCE)0733-9429(1996)122:10(549)

van Rijn, L.C., 1984. Sediment transport part II, suspended load transport. Journal of Hydraulic Engineering-ASCE, 110 (11): 1613–1641. DOI:http://dx.doi.org/10.1061/(ASCE)0733-9429(1984)110:11(1613)

Villanueva, I., Wright, N.G., 2006. Linking Riemann and storage cell models for flood prediction. Proceedings of the ICE - Water Management, 159(1): 27-33. DOI:10.1680/wama.2006.159.1.27

Westoby, M.J. et al., 2014. Modelling outburst floods from moraine-dammed glacial lakes. Earth-Science Reviews, 134(0): 137-159. DOI:http://dx.doi.org/10.1016/j.earscirev.2014.03.009

Wong, J.S., Freer, J.E., Bates, P.D., Sear, D.A., Stephens, E.M., 2014. Sensitivity of a hydraulic model to channel erosion uncertainty during extreme flooding. Hydrological Processes. DOI:10.1002/hyp.10148

Wu, W., 2004. Depth-averaged two-dimensional numerical modeling of unsteady flow and nonuniform sediment transport in open channels. Journal of Hydraulic Engineering-ASCE, 130(10): 1013-1024. DOI:http://dx.doi.org/10.1061/(ASCE)0733-9429(2004)130:10(1013))

Wu, W., Rodi, W., Wenka, T., 2000. 3D numerical modeling of flow and sediment transport in open channels. Journal of Hydraulic Engineering, 126(1): 4-15.

Yang, H., Lin, B., Zhou, J., 2015. Physics-based numerical modelling of large braided rivers dominated by suspended sediment. Hydrological Processes, 29(8): 1925-1941. DOI:10.1002/hyp.10314

Zech, Y., Soares-Frazao, S., Spinewine, B., Grelle, N.L., 2008. Dam-break induced sediment movement: Experimental approaches and numerical modelling. Journal of Hydraulic Research, 46(2): 176-190. DOI:10.1080/00221686.2008.9521854

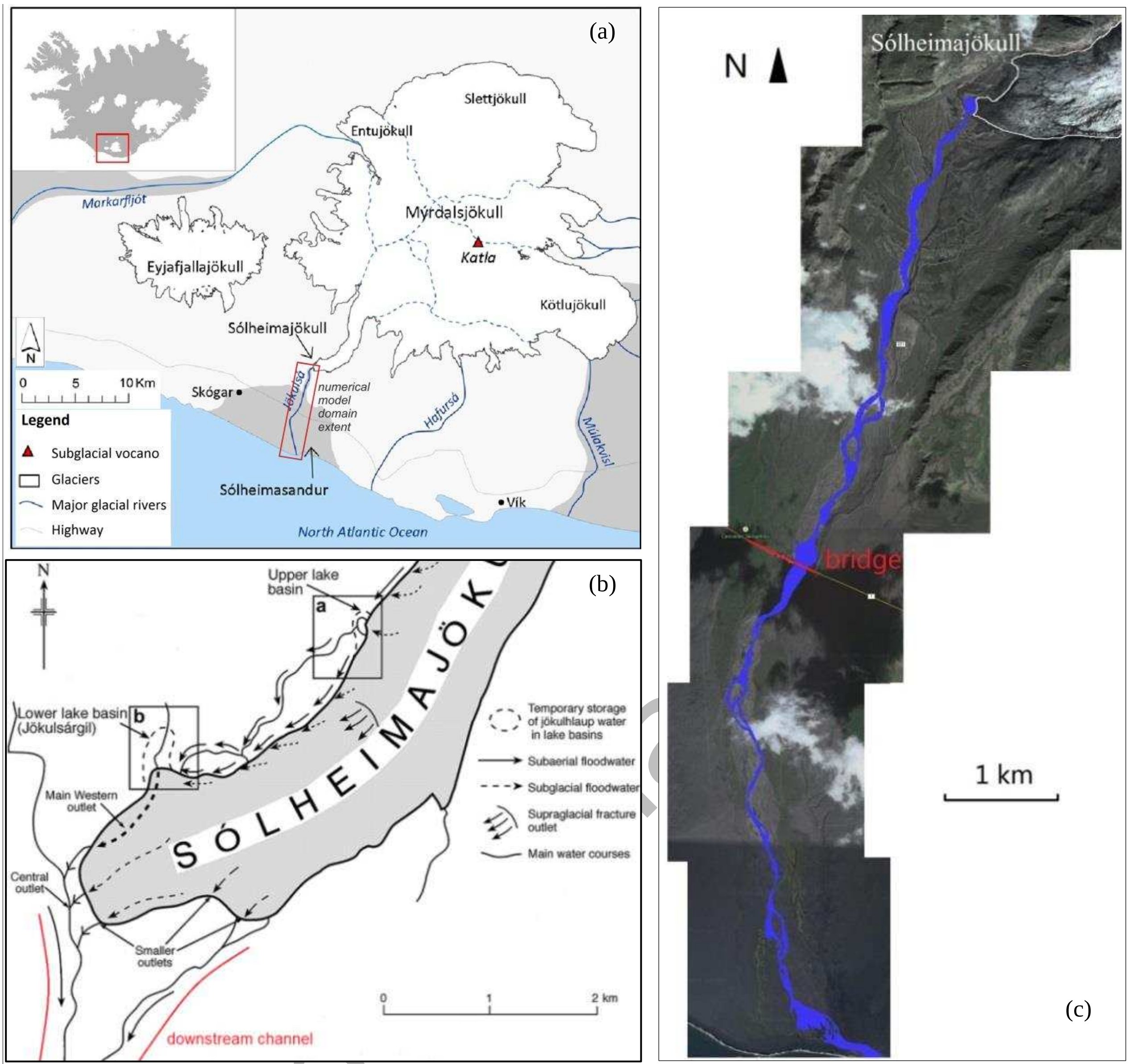

Fig. 1. (a) The location of the glacier, (b) the July 1999 flood route ways and temporary floodwater storage locations (Russell et al., 2010), (c) the studied river channel for numerical modelling

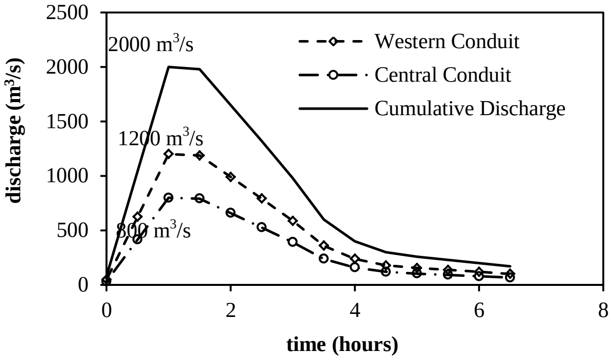

Fig. 2 The hydrograph from Western Conduit, Central Conduit and cumulative inflow discharge

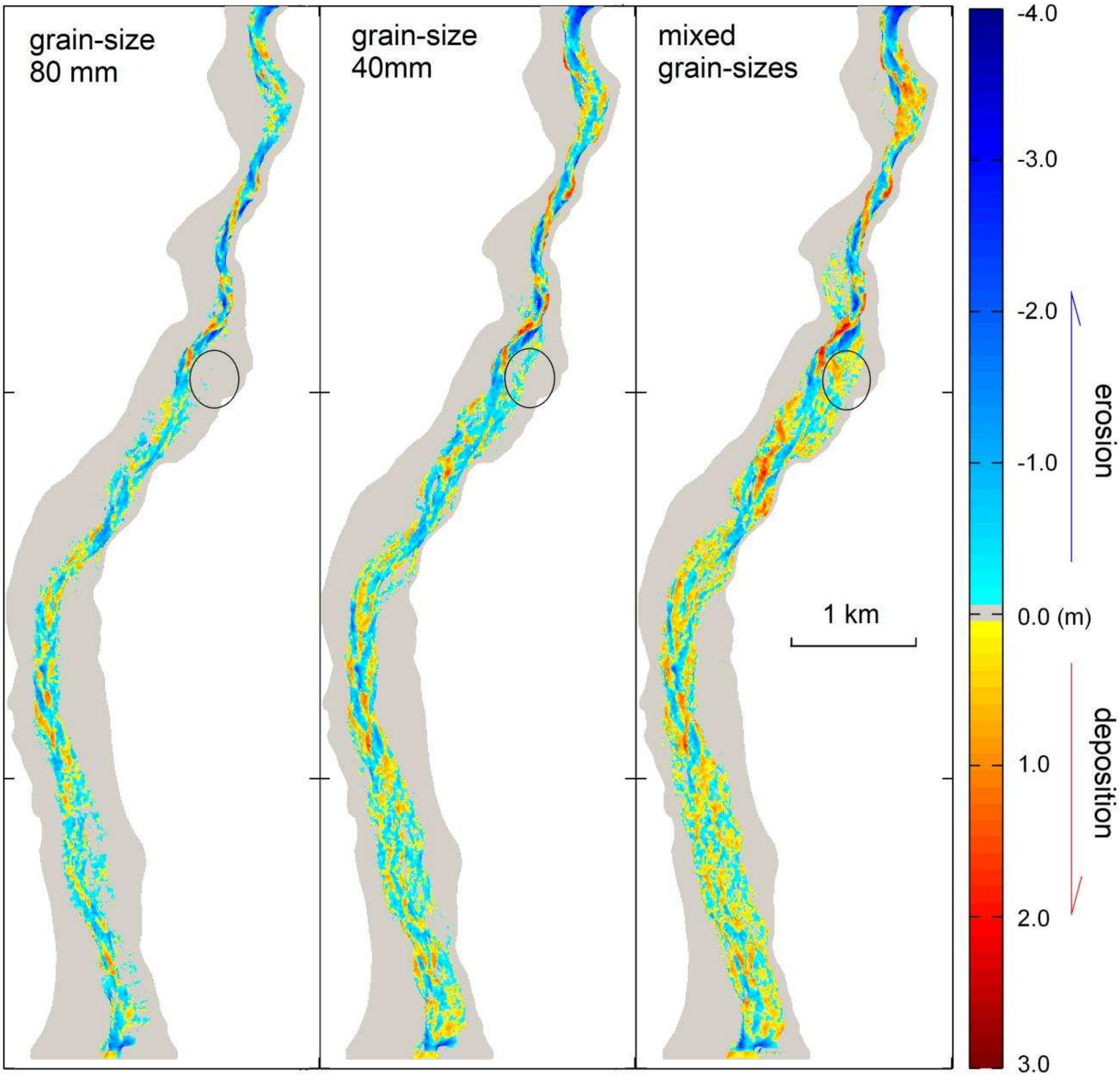

Fig. 3. The simulated spatial distribution of net bed erosion and deposition for the three parameterisations of grain-size

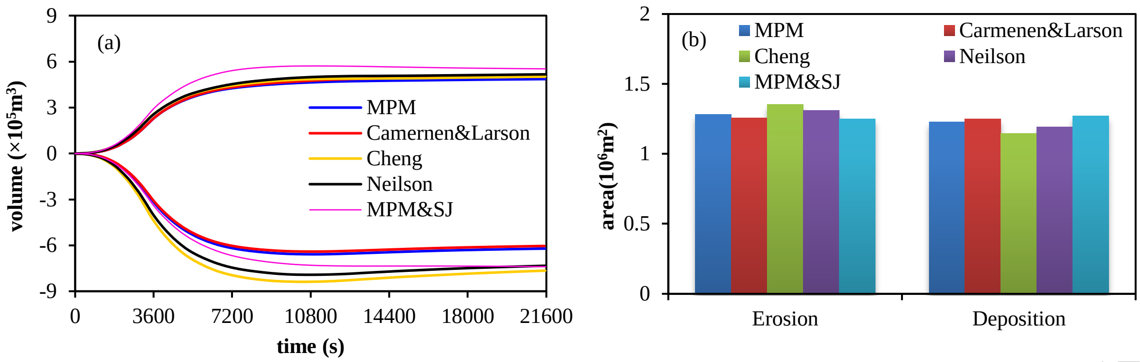

Fig. 4. (a) Temporal changes of modelled erosion and deposition volumes, note: negative values denotes erosion volume, positive value represents deposition volume, and (b) the final erosion area and deposition area in the river channel

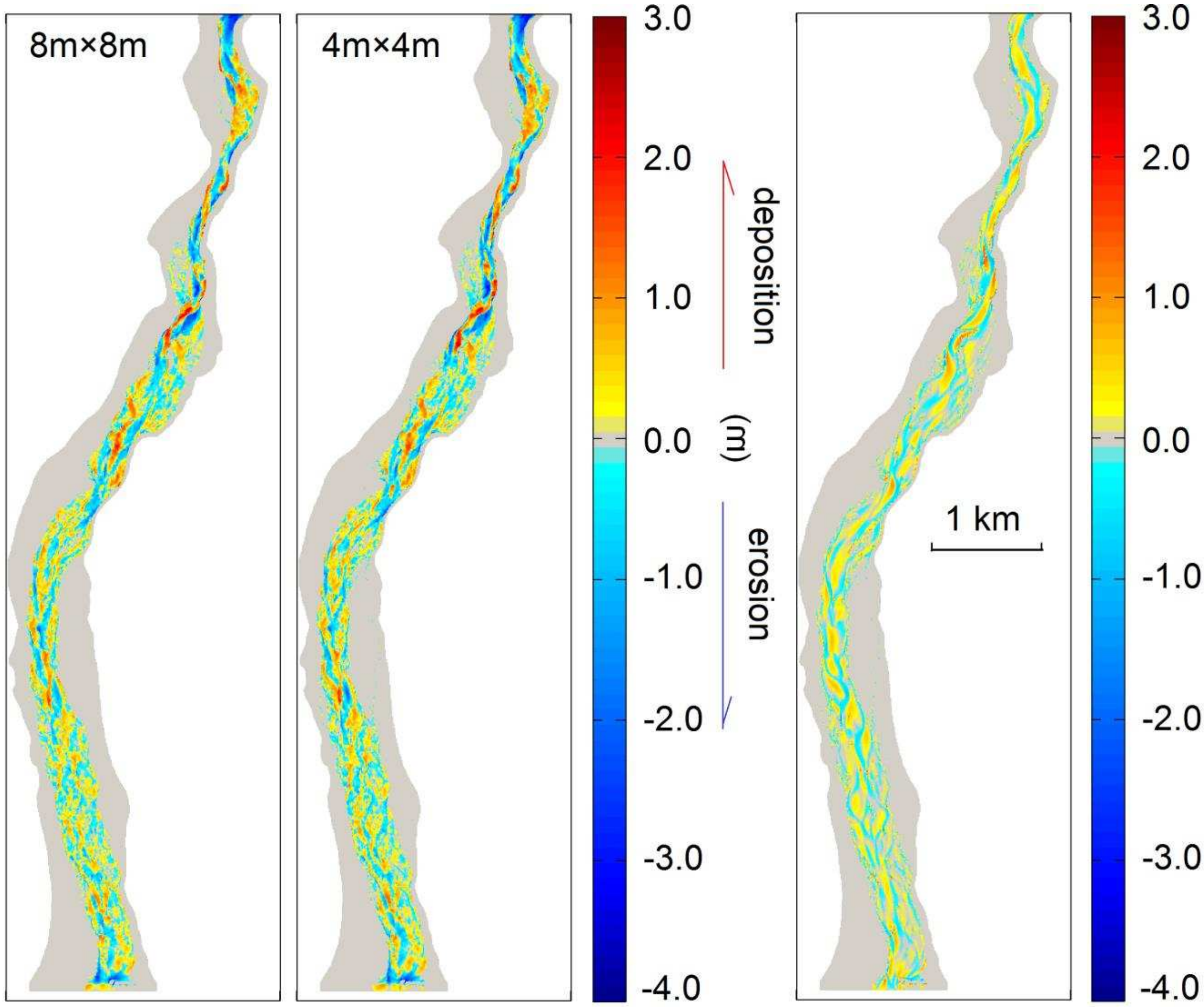

Fig. 5. Spatial pattern of modelled erosion and deposition for the simulations with DEMs of 4m×4m and 8m×8m, and the difference between the two runs (DEM with 4m×4m minus DEM with 8m×8m)

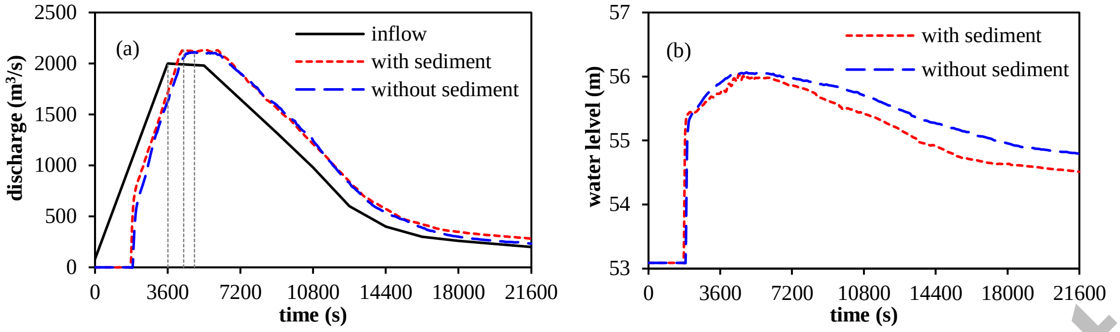

Fig. 6. (a) The temporal change of flow discharge at the cross section x=332908.86; and (b) the temporal change of water depth at the gauge (332908.86, 480099.78)

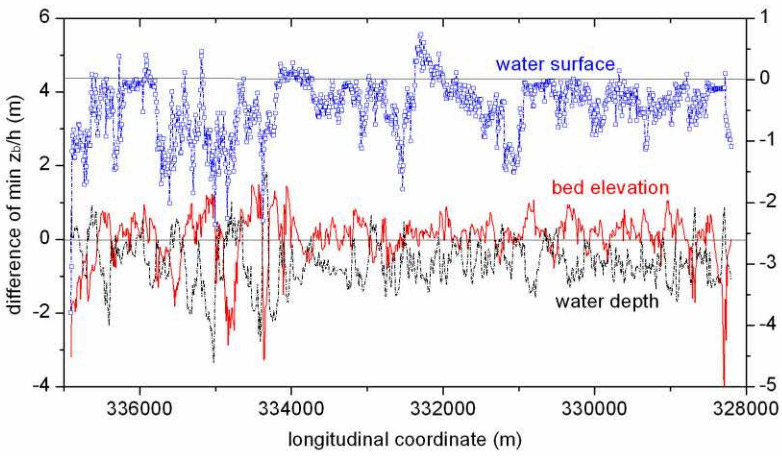

Fig. 7. The differences of the modelled results with and without the inclusion of sediment transport, including the minimum water level, the minimum water depth, and the minimum bed elevation; herein $\Delta\eta = \eta_{sed} - \eta_{no\,sed}$, $\Delta h = h_{sed} - h_{no\,sed}$, $\Delta z = z_{sed} - z_{no\,sed}$

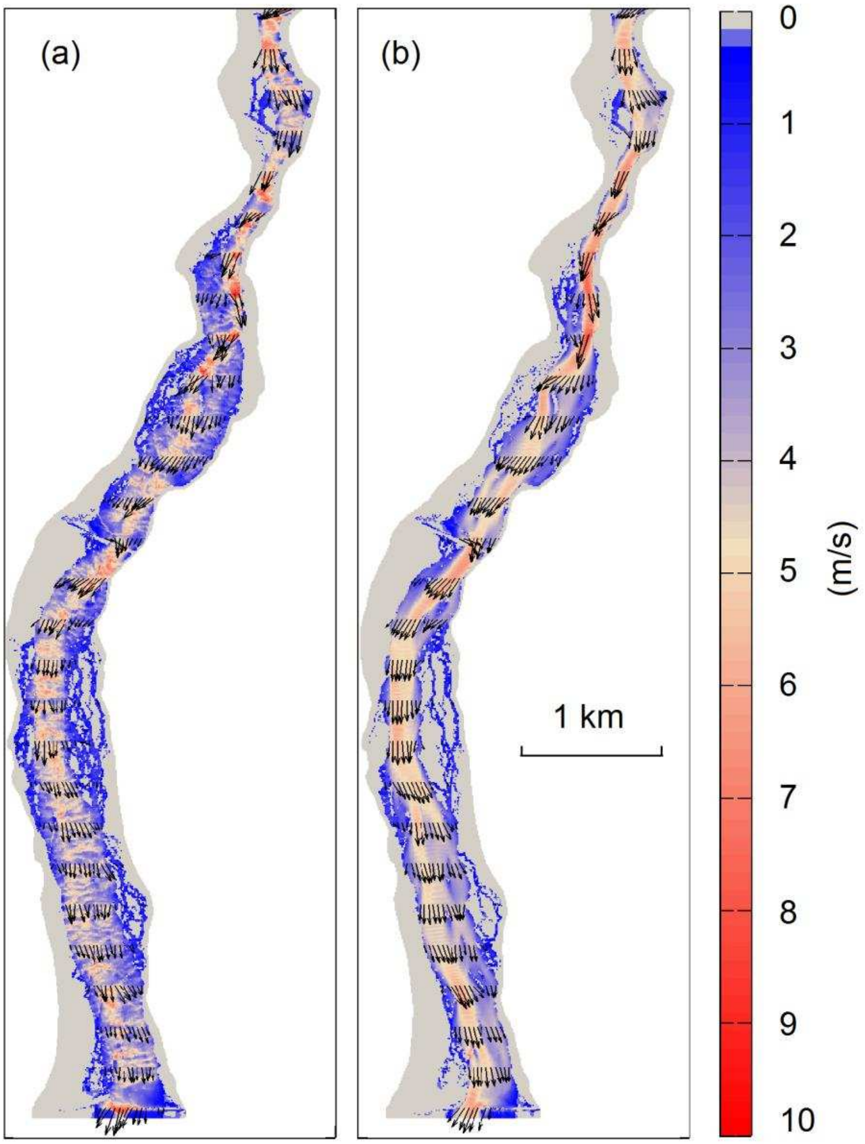

Fig. 8. The spatial pattern of the modelled velocity field, and the velocity vectors at some cross-sections with and without the consideration of geomorphological changes at the peak stage t = 2 hours; (a) the modelled result without morphological changes, (b) the modelled results with morphological changes

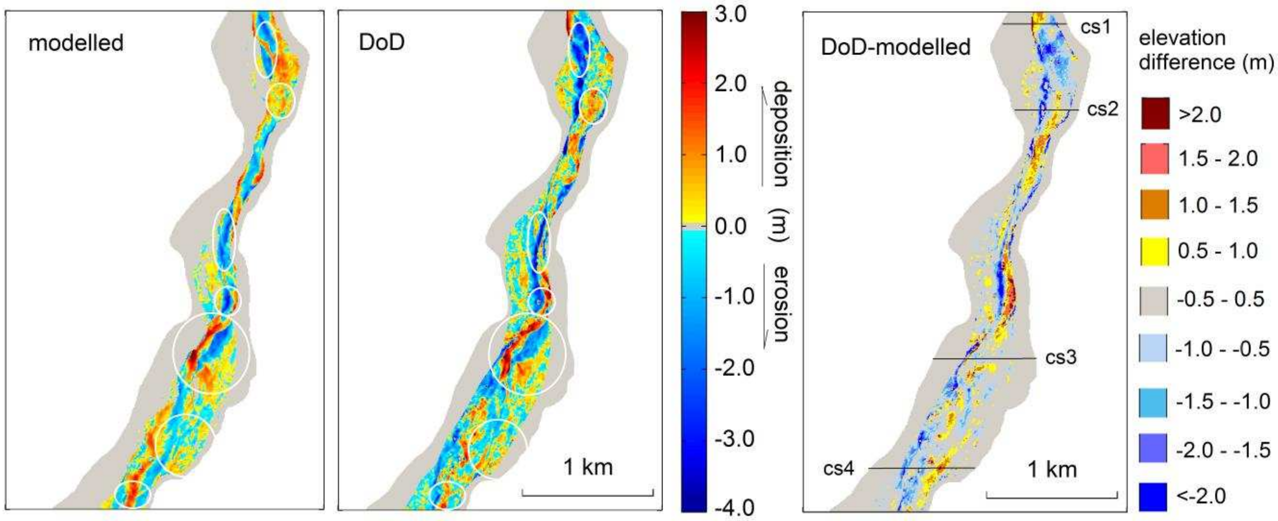

Fig. 9. Comparison of the modelled bed changes (a) and the measured differenced DEM between the pre-flood DEM and the post-flood DEM (b), and (c) the elevation difference between the modelled and the measured bed changes (measured bed minus modelled bed); the while circles represent several highlight zones.

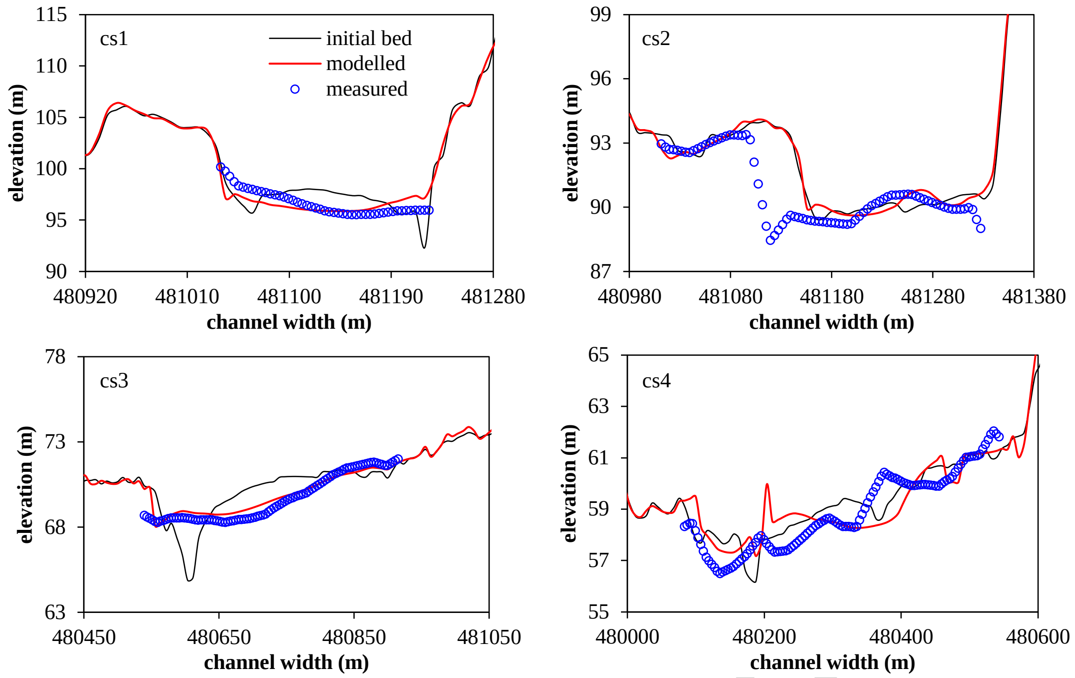

Fig. 10. Comparison of the modelled bed profiles and the measured ones at the four cross-sections shown in Fig. 9(c).

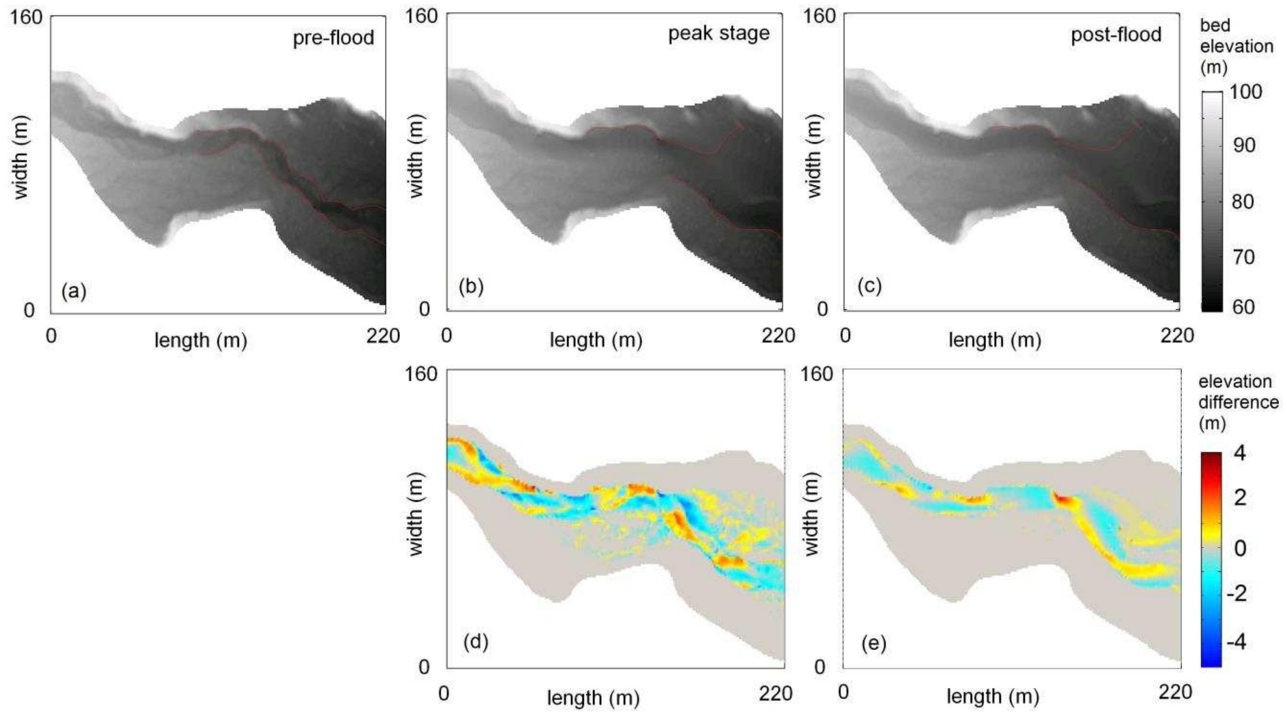

Fig. 11. Bed elevation of a short reach near the bridge (a) before flood; (b) at peak stage; (c) after flood; as well as the difference of bed elevation between each other, (d) = (b) – (a), (e) = (c) – (b)

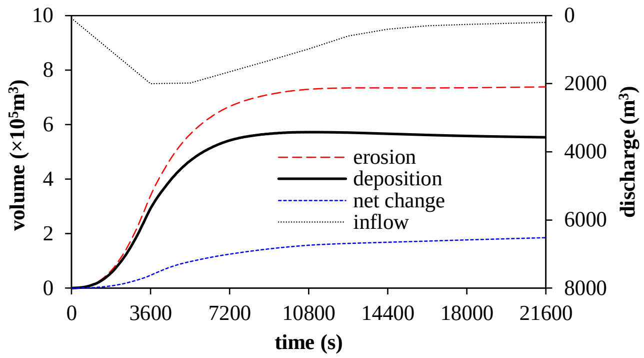

Fig. 12. Temporal volume evolution for total erosion, deposition, and net riverbed change (erosion minus deposition)

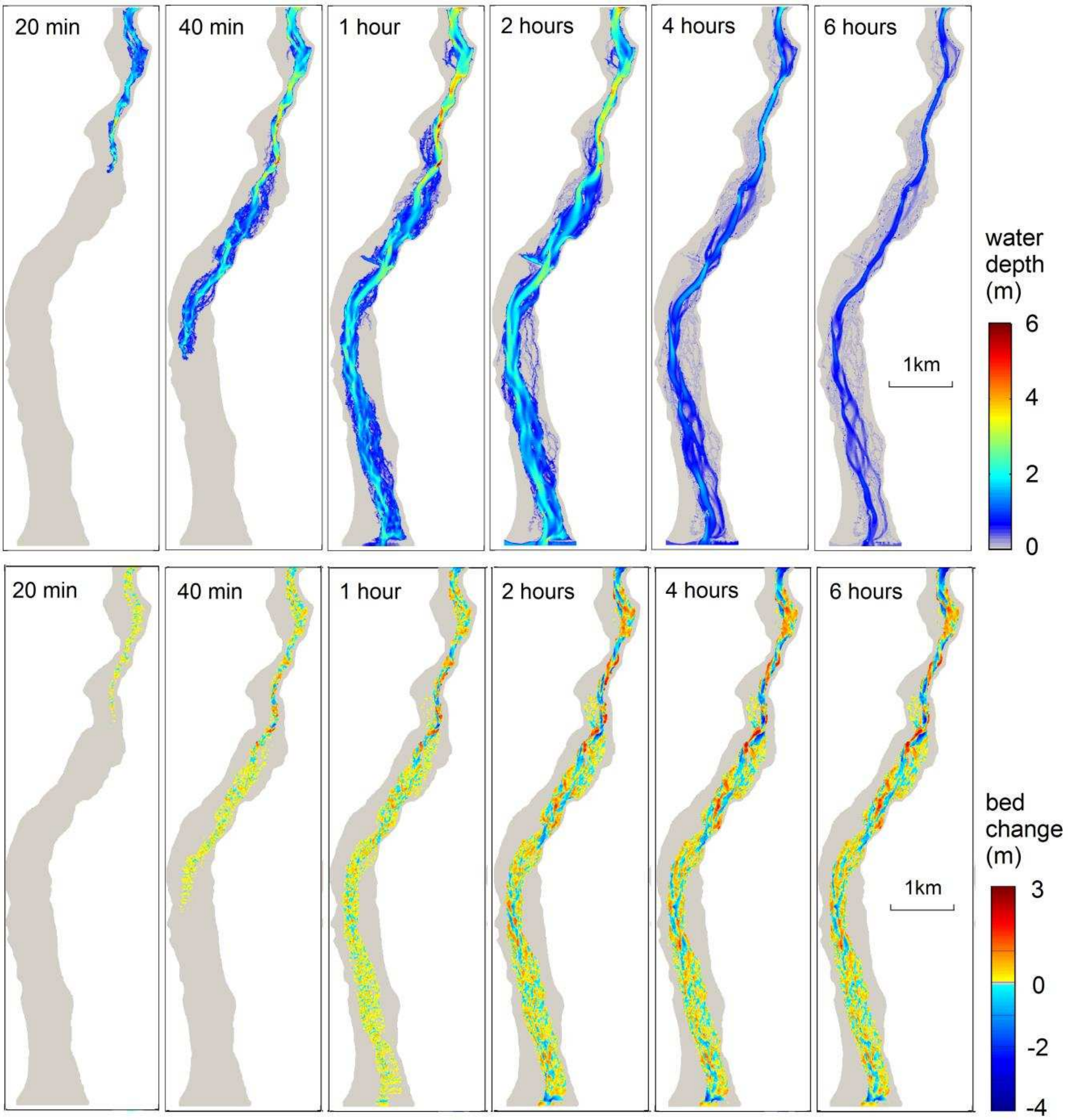

Fig. 13. Spatial pattern of the modelled water depth (the upper row) and bed changes (the lower row) at 20 min, 40 min, 1 hour, 2 hours, 4 hours and 6 hours after the flood initiation; note: for the bed changes, negative value denotes erosion depth, and positive value represents deposition depth